Case Studies in Thermal Engineering 32 (2022) 101893

Contents lists available at ScienceDirect

Case Studies in Thermal Engineering

journal homepage: www.elsevier.com/locate/csite

Heat and mass transfer analysis of nonlinear mixed convective hybrid nanofluid flow with multiple slip boundary conditions

Wei-Feng Xia [a], Shafiq Ahmad [b,*], Muhammad Naveed Khan [b], Hijaz Ahmad [c,**], Aysha Rehman [d], Jamel Baili [e,f], Tuan Nguyen Gia [g]

[a] School of Engineering, Huzhou University, Huzhou, 313000, PR China
[b] Department of Mathematics, Quaid-I-Azam University, Islamabad, Pakistan
[c] Section of Mathematics, International Telematic University Uninettuno, Corso Vittorio Emanuele II, 39, 00186, Roma, Italy
[d] Department of Mathematics, University of Gujrat, Gujrat, 50700, Pakistan
[e] Department of Computer Engineering, College of Computer Science, King Khalid University, Abha, 61413, Saudi Arabia
[f] Higher Institute of Applied Science and Technology of Sousse (ISSATS), Cité Taffala (Ibn Khaldoun) 4003 Sousse, University of Souse, Tunisia
[g] Department of Computing, University of Turku, 20500, Turku, Finland

ARTICLE INFO

Keywords:
Hall Current
Hybrid nanofluid (CNTs+ refrigerant-134A)
Nonlinear mixed convection
Joule heating
Slendering sheet
Gyrotactic-microorganism

ABSTRACT

The current study focuses on the 3D nonlinear mixed convective boundary layer flow of micropolar hybrid nanofluid in the presence microorganism and multiple slip conditions across the slendering surface. The concentration and energy equations are developed in the occurrence of activation energy and joule heating effect. The aim of this research is to consider the Carbon nanotubes (CNTs) which are favored materials in the manufacture of electrochemical devices because of their mechanical and chemical stability, good thermal and electrical conductivities, physiochemical consistency, and featherweight. By keeping such extraordinary properties of carbon nanotubes in mind, we investigate the flow of hybrid nanofluid having MWCNT (multi-wall carbon nanotubes) and SWCNT (single-wall carbon nanotubes). Using an appropriate similarity variable, the flow model (PDEs) are converted into nonlinear ordinary differential equations. The bvp4c approach is utilized to tackle the coupled differential equations. The impact of emerging parameter on temperature distribution, velocity field, concentration distribution, and microorganism field are presented graphically. It is noted the stronger values of wall thickness parameter and Hartmann number produces retardation effect, as a result fluid velocity declines for both SWCNT (single-wall carbon nanotubes) and MWCNT (multi-wall carbon nanotubes) hybrid nanofluid. Furthermore, the transport rate of heat and mass improves by the higher values of φ_2 for both simple and hybrid nanofluid.

1. Introduction

Nanoparticles have risen in importance due to their numerous applications in thermal transport, heat exchangers, thermal power plants, microelectronics, and microelectronic system technology. In comparison to regular liquids such as oil, propylene glycol, ethylene glycol, and water nanomaterial have a high thermal efficiency. The injection of nanomaterials into pure liquids (coolants) improves their thermal conduction ability. Nanoliquids are a mixture of nanoparticles (1–100 nm) in size and base fluid. Thermo-

* Corresponding author.
** Corresponding author.
E-mail addresses: ashafiq@math.qau.edu.pk (S. Ahmad), hijaz555@gmail.com (H. Ahmad).

https://doi.org/10.1016/j.csite.2022.101893
Received 13 June 2021; Received in revised form 20 September 2021; Accepted 19 February 2022
Available online 22 February 2022

physical features and volume fraction of nanoparticles are used to determine the heat transfer characteristics of Nanoliquids. Carbides, fullerene, Oxides, nitrides, metals, and carbon nanotubes are among the different groups of nanomaterials categorized based on their shapes, sizes, and properties. Carbon nanotubes are cylindrical shaped tubes with invaluable properties such as immense potency and strong thermal conductivity, which making them extremely attractive materials in a variety of fields such as optics, drug delivery, microwave amplifiers, health care, prostheses, environment, and nanotube transistors, and many other fields [1–5]. Carbon nanotubes are categorized into two categories: multi-wall carbon nanotubes (MWCNTs) and single-wall carbon nanotubes (SWCNTs). Lijima first invented carbon nanotubes (CNTs) in 1991. He used the Krastschmer and Huffman process for the first time to review multi-walled carbon nanotubes (MWCNTs). In addition, Donald Bethune published single-walled carbon nanotubes (SWCNT) in 1993. In their research, Ramasubramaniam et al. [6] discovered that SWCNTs are very useful in electrical conductivity implementations. Composite nanotubes, according to Xue [7], are crucial for increasing thermal conductivity. Kumar et al. [8] evaluated three-dimensional magnetohydrodynamic convective mass and heat transport of nanofluid across a slendering stretching layer embedded in a porous medium along concentration and temperature slip mechanisms, as well as a heat source/sink. The enhancement in the transport of heat transfer in the occurrence of 3D micropolar hybrid nanofluid with porous medium across an exponentially stretching surface is scrutinized by Manjunatha et al. [9]. Ramesh et al. [10] explored the mixed convection flow of viscous hybrid nanofluid across a vertical porous cylinder with heterogeneous and homogeneous reactions. Recent research in the area of nanofluids can be seen in Refs. [11–15].

Slendering stretching surface has more features in engineering processes than linear stretching sheet, including hot rolling, glass-fiber manufacturing, melt-spinning, petroleum production, metallic plate cooling in a bath, extrusion, polymer sheet extraction, rubber and plastic sheet production, wire drawing, that might be an electrolyte, and so on. Due to the observable importance application, Babu and Sandeep [16] investigated non-Newtonian fluid flow against a slendering stretching layer with multiple slip and magnetic field impact. In the existence of Hall current effect, viscous dissipation, and Arrhenius activation energy, Nandi et al. [17] investigated the 3D radiative Williamson fluid flow with Brownian effect through a variable thickness stretching surface. Devi and Prakash [18] numerically observed the hydromagnetic fluid flow along slip and variable magnetic field effects. The magnetohydrodynamics (MHD) Casson fluid flow across a slendering stretching sheet is analyzed by Akolade et al. [19] with the influence of multi slips and Soret–Dufour. As heat generation, thermal radiation, and Newtonian heating impact were taken into account, Qayyum et al. [20] to observe nanofluid flow towards a slendering stretching surface. Reddy et al. [21] explored the heat transport enhancement in the Magnetite nanoliquid through a variable thickness stretching surface in the appearance of thermal radiation and viscous dissipation. More studies are found in Refs. [22–26] about slendering stretching surface.

Mixed convection flow behaviors across a stretching surface have a wide spectrum of uses in industry and engineering. In the existence of gravitational force, free convection effect becomes more important. Both stretching and buoyancy forces influence the flow and heat transfer mechanisms. Thermal buoyancy forces are generated when the temperature of the stretching surface changes, affecting the rate of heat transfer in industrial processes. Electronic device cooling, heat exchangers in low-velocity environments, boilers, nuclear reactor cooling through emergency shutdown, solar energy systems, defroster system, flows in the atmosphere, vehicle demister, and ocean are all affected by this phenomenon. Mixed convection radiative flow across a porous inclined plate is characterized by Moradi et al. [27]. In the existence of double stratification and activation energy Ahmad et al. [28] deliberated the mixed convection hybrid nanofluid flow through an exponentially stretched surface. Elsaid et al. [29] reported mixed convective flow of a hybrid nanofluid passing towards a vertical channel along variable temperature and thermal radiative flux. The study of MHD radiating hybrid nanofluid ($Ag - TiO_2 - H_2O$) flow with homogeneous-heterogeneous reactions through a thin needle is probed by Puneeth et al. [30]. Nadeem et al. [31] numerically scrutinized the CNTs impact in the stagnation point flow in the occurrence of mixed convection, heat generation, and Thomson and Troian slip condition along a Riga plate.

One of the fascinating impacts to be exerted is joule heating, which has a significant impact on MHD fluid flow. Joule heating (Ohmic heating) is a method of conversion energy from electric to thermal, which generates heat across resisting deficiencies in the material. The Ohmic heating (Joule heating) phenomenon is also usually used in electric and electronic devices. Reddy and Reddy [32] investigated the impact of Joule heating and Brownian motion in a peristaltic flow along the compliant walls. Reddy says that the temperature might be raises due to occurrence of Joule heating. Analysis of transfer of heat in carbon nanotube-based systems Hayat et al. [33] investigate radiative Darcy–Forchheimer flow across a curved stretching surface influenced by Joule heating and viscous dissipation. Ghadikolaei et al. [34] numerically analyzed the MHD flow of CNTs-water hybridnanofluid as a non-Newtonian micropolar dusty nanofluid, which was affected by joule heating and linear thermal radiation above a stretching plate. In the occurrence of viscous dissipation and Joule heating, the hybrid nanofluid flow past a rotational disk is deliberated by Shoaib et al. [35]. Ijaz et al. [36] numerically investigated the activation energy impact for the Walter-B nanoparticle model in the existence of Ohmic heating (Joule heating) across a stretching surface. More recent studies about Joule heating are discussed in Refs. [37–40].

As a result of all the above research, the current research numerically explores the effects of hybrid nanofluid on a MHD mixed convective flow against a slendering stretching sheet with Hall current, viscous dissipation, and Joule heating. The appearance of a hybrid nanofluid comprising SWCNT and MWCNT with refrigerant-134A as a regular fluid and gyrotactic microorganisms is a major contribution to this study. This is the first analysis of such kind, and it will be good contribution in the literature about hybrid nanofluid flows. The comparative study between simple and hybrid nanofluid through graphs are examined in the whole results. The flow model is converted to nonlinear ODEs using the similarity variables and tackled numerically by employing MATLAB bvp4c approach [41–43]. The numerical values of local skin friction coefficients, motile density of microorganism, as well as local mass and heat transfer rate are discussed with tabulated data. Furthermore, the findings are validated by comparing them to previously published material in the literature, which is a notable feature of the present results. In this aspect, a venerable stability has been accomplished.

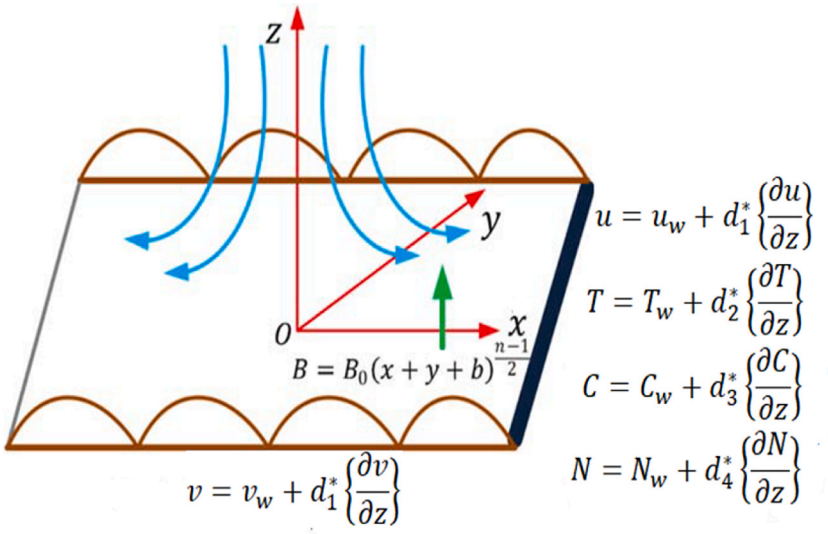

Fig. 1. Flow diagram of the problem.

2. Formulation of the problem

Here, we investigate 3D, laminar, incompressible, steady, and nonlinear mixed convective flow of hybrid nanofluid flow with microorganism over a slendering surface. The multiple slip conditions are implemented on the boundary of the surface. The transport of heat and mass is explored in the presence of joule heating, viscous dissipation, activation energy, and Hall current effect respectively. The flow diagram for the present problem is shown in Fig. 1. The flow is constrained to the z ≥ 0 region. In the z-direction, the magnetic field is applied. The $u_w = u_0(y+x+b)^n$, and $v_w = v_0(y+x+b)^n$ are the stretching velocities in the x- and y-directions, respectively. The fluid temperature, concentration, and microorganism density are considered by T, C, and N respectively. Further, the wall temperature, concentration, microorganism density are indicated by T_w, C_w, and N_w respectively, and in the ambient form they are signified by T_∞, C_∞, and N_∞ respectively. The present model assumes a velocity $V = (u(x,y,z),\ v(x,y,z),\ w(x,y,z))$. By the considering above suppositions, the obtaining equation of mass, momentum, concentration, temperature, and microorganism are identified as [22],

$$\frac{\partial v}{\partial y}+\frac{\partial u}{\partial x}+\frac{\partial w}{\partial z}=0, \tag{1}$$

$$v\frac{\partial u}{\partial y}+u\frac{\partial u}{\partial x}+w\frac{\partial u}{\partial z}=\nu_{hnf}\frac{\partial^2 u}{\partial z^2}+g^*\left\{\begin{array}{l}(T-T_\infty)(\gamma_1+\gamma_2(T-T_\infty))\\+\gamma_3(C-C_\infty)+\gamma_4(C-C_\infty)^2\\+\gamma_5(N-N_\infty)+\gamma_6(N-N_\infty)^2\end{array}\right\}-\frac{\sigma_{hnf}B^2}{\rho_{hnf}(1+m^2)}(u+mv)\ , \tag{2}$$

$$u\frac{\partial v}{\partial x}+v\frac{\partial v}{\partial y}+w\frac{\partial v}{\partial z}=\nu_{hnf}\frac{\partial^2 v}{\partial z^2}-\frac{\sigma_{hnf}B^2}{\rho_{hnf}(1+m^2)}(v-mu)\ , \tag{3}$$

$$v\frac{\partial T}{\partial y}+u\frac{\partial T}{\partial x}+w\frac{\partial T}{\partial z}=\frac{\sigma_{hnf}B_0^2}{(\rho C_p)_{hnf}(1+m^2)}(u^2+v^2)+\alpha_{hnf}\frac{\partial^2 T}{\partial z^2}+\frac{\mu_{hnf}}{(\rho C_p)_{hnf}}\left(\left(\frac{\partial v}{\partial z}\right)^2+\left(\frac{\partial u}{\partial z}\right)^2\right), \tag{4}$$

$$u\frac{\partial C}{\partial x}+v\frac{\partial C}{\partial y}+w\frac{\partial C}{\partial z}+\Lambda^2(C-C_\infty)\left(\frac{T}{T_\infty}\right)^{n_1}\exp\left(\frac{-E_a}{k_1^*T}\right)=(D_B)_{hnf}\frac{\partial^2 C}{\partial z^2}, \tag{5}$$

$$u\frac{\partial N}{\partial x}+v\frac{\partial N}{\partial y}+w\frac{\partial N}{\partial z}=(D_N)_{hnf}\frac{\partial^2 N}{\partial z^2}-\frac{\widetilde{b}W_c}{(C_w-C_\infty)}\frac{\partial}{\partial z}\left(N\frac{\partial C}{\partial z}\right). \tag{6}$$

The convenient boundary conditions are defined in the form [16],

$$\left.\begin{array}{l}u=d_1^*\frac{\partial u}{\partial z}+u_w,\ v=d_1^*\frac{\partial v}{\partial z}+v_w,\ w=0,\quad T=d_2^*\frac{\partial T}{\partial z}+T_w,\\C=d_3^*\frac{\partial C}{\partial z}+C_w,\ N=d_4^*\frac{\partial N}{\partial z}+N_w.\end{array}\right\}\ at\ \ z=j(b+x+y)^{\frac{1-n}{2}}. \tag{7}$$

$$u\to 0,\ T\to T_\infty, v\to 0,\ C\to C_\infty,\ at\ z\to\infty. \tag{8}$$

Table 1
Thermophysical features of the nanoparticles and base fluid [41, 43].

Physical characteristics	Nanoparticles		Base fluid
	SWCNTs	MWCNTs	$C_2H_2F_4$
ρ (kg m^{-3})	2600	1600	1199.7
C_p (J kg^{-1}/K)	425	796	1432
k (Wm^{-1}/K)	6600	3000	0.0803

In Eqs. 2–10, the symbols g^*, ν_{hnf}, (γ_1, γ_2), σ_{hnf}, α_{hnf}, ρ_{hnf}, μ_{hnf}, C_p, (γ_3, γ_4), $(D_B)_{hnf}$, $(D_n)_{hnf}$, W_c, $\widetilde{b}$, Λ, k^*, m, (γ_5, γ_6), n, and E_a are represented the gravitational acceleration, kinematics viscosity, linear and non-linear thermal expansion, electrical conductivity, thermal diffusivity, dynamic viscosity, specific heat, linear and non-linear concentration expansion, mass diffusivity, microorganism diffusivity, cell swimming speed, chemotaxis constant, chemical reaction constant, mean absorption coefficient, hall current parameter, linear and non-linear microorganism expansion, power law index, and activation energy constant, respectively. Further, d_1^*, d_2^*, d_3^*, and d_4^* are the velocity slip, thermal slip, concentration slip, and microorganism slip factors, respectively. Table 1 summarizes the thermophysical characteristics of the basic liquid ($C_2H_2F_4$), as well as nanoparticles like SWCNTs and MWCNTs.

2.1. Model of nanofluid and hybrid nanofluid

Below are the reported statements of nanofluid and hybrid nanofluid [31, 41, 43].

Physical characteristics	$SWCNT - C_2H_2F_4$
μ (Viscosity)	$\mu_{nf} = \mu_f(1-\varphi)^{-2.5}$,
k (conductivity)	$\frac{k_{nf}}{k_f} = \frac{k_{SWCNT} - (1-n)k_{C_2H_2F_4} + (1-n)\varphi(k_{C_2H_2F_4} - k_{SWCNT})}{k_{SWCNT} - (1-n)k_{C_2H_2F_4} + \varphi(k_{C_2H_2F_4} - k_{SWCNT})}$,
ρ (Density)	$\rho_{nf} = \varphi\rho_{SWCNT} + (1-\varphi)\rho_{C_2H_2F_4}$,
ρC_p (Heat capacity)	$(\rho C_p)_{nf} = (\rho C_p)_{SWCNT}\varphi + (\rho C_p)_{C_2H_2F_4}(1-\varphi)$,
Physical characteristics	$MWCNT - SWCNT - C_2H_2F_4$
μ (Viscosity)	$\mu_{hnf} = \mu_f \Big/ (1-\varphi_1)^{25/10}(1-\varphi_2)^{25/10}$,
ρ (Density)	$\rho_{hnf} = \{\rho_{s1}\varphi_1(1-\varphi_2) + (1-\varphi_1)(1-\varphi_2)(\rho_f)\} + \rho_{s2}\varphi_2$,
ρC_p (Heat capacity)	$(\rho C_p)_{hnf} = (\rho C_p)_{s2}\varphi_2 - (\varphi_2 - 1)\{(\rho C_p)_{s1}\varphi_1 + (1-\varphi_1)((\rho C_p)_f)\}$,
k (Thermal conductivity)	$\frac{k_{hnf}}{k_{bf}} = \frac{(1-\varphi_2) + 2\varphi_2\left(\frac{k_{SWCNT}}{k_{SWCNT}-k_{bf}}\right)\ln\left(\frac{k_{SWCNT}+k_{bf}}{k_{bf}}\right)}{(1-\varphi_2) + 2\varphi_2\left(\frac{k_{bf}}{k_{SWCNT}-k_{bf}}\right)\ln\left(\frac{k_{SWCNT}+k_{bf}}{k_{bf}}\right)}$,
	$\frac{k_{bf}}{k_f} = \frac{(1-\varphi_1) + 2\varphi_1\left(\frac{k_{MWCNT}}{k_{MWCNT}-k_f}\right)\ln\left(\frac{k_{MWCNT}+k_f}{k_f}\right)}{(1-\varphi_1) + 2\varphi_1\left(\frac{k_f}{k_{MWCNT}-k_f}\right)\ln\left(\frac{k_{MWCNT}+k_f}{k_f}\right)}$.

The subscript identifies the solid particles SWCNT (s_2) and MWCNT (s_1) as per the above properties.

2.2. Similarity transformation

The relevant similarity transformations are given as follows [16],

$$\begin{aligned}
&\eta = z\left(\frac{u_0}{\nu_f}\right)^{\frac{1}{2}}(b+y+x)^{\frac{n-1}{2}},\ u = u_0(b+y+x)^n F'(\eta),\ v = u_0(b+y+x)^n G'(\eta),\\
&w = -\left(u_0\nu_f\right)^{\frac{1}{2}}(b+y+x)^{\frac{n-1}{2}}\left(\frac{n+1}{2}(G(\eta)+F(\eta)) - \eta\frac{1-n}{2}(G'(\eta)+F'(\eta))\right),\\
&T - T_\infty = (T_w - T_\infty)\theta(\eta),\ C - C_\infty = (C_w\overline{\varepsilon}(\eta) - C_\infty\overline{\varepsilon}(\eta)),\ N - N_\infty = (N_w H(\eta) - N_\infty H(\eta)).
\end{aligned} \tag{9}$$

The wall velocity, temperature, concentration, and microorganism density are stated as,

$$\begin{aligned}
&u_w = u_0(b+y+x)^n,\ v_w = v_0(b+y+x)^n,\ T_w = T_\infty + T_0(b+y+x)^{\frac{1-n}{2}},\ \Lambda^2 = K_0^2(b+y+x)^{n-1}\\
&B = B_0(b+y+x)^{\frac{1-n}{2}},\ C_w - C_\infty = C_0(b+y+x)^{\frac{1-n}{2}},\ N_w - N_\infty = N_0(b+y+x)^{\frac{1-n}{2}}.
\end{aligned} \tag{10}$$

Using above transformations, the equations $(2)-(10)$ in dimensionless form,

$$\begin{aligned}
&F''' + A_1A_2\left(\frac{n+1}{2}\right)(F+G)F'' - \frac{HaA_2\sigma_{hnf}}{(1+m^2)\sigma_f}(F'+mG') + A_2\lambda(1+\lambda_1\theta)\theta\\
&+A_2\lambda N_r(1+\lambda_2\overline{\varepsilon})\overline{\varepsilon} + A_2\lambda N_c(1+\lambda_3 H)H - A_1A_2(nF'+nG')F' = 0,
\end{aligned} \tag{11}$$

$$G''' + 2A_1A_2\left(\frac{n+1}{2}\right)\left(\frac{F+G}{2}\right)G'' + \frac{HaA_2\sigma_{hnf}}{(1+m^2)\sigma_f}(mF' - G') - nA_1A_2(F' + G')G' = 0, \tag{12}$$

$$\frac{k_{hnf}}{k_f}\theta'' + \mathrm{Pr}A_3\left[\begin{array}{l}\frac{\sigma_{hnf}HaEc}{\sigma_f A_3\left(1+m^2\right)}\left(F'2 + G'2\right) \\ +\left(\frac{n+1}{2}\right)(F+G)\theta'\end{array}\right] + \frac{Ec\mathrm{Pr}}{A_2}\left(F'2 + G'2\right) = 0, \tag{13}$$

$$\frac{A_2}{S_c}\bar{\varepsilon}'' + \left(\frac{n+1}{2}\right)(F+G)\bar{\varepsilon}' - K_r\bar{\varepsilon}(1+\delta\theta)^{n_1}\exp\left(\frac{-E}{1+\delta\theta}\right) = 0, \tag{14}$$

$$\frac{A_2}{S_b}H'' + \left(\frac{n+1}{2}\right)(F+G)H' - \frac{P_e}{S_b}((H+\Omega)\bar{\varepsilon}'' + H'\bar{\varepsilon}') = 0. \tag{15}$$

The convenient boundary conditions become,

$$\left.\begin{array}{l} F = \alpha_1\left(\frac{1-n}{1+n}\right)(1 + K_1F''),\ G = \alpha_1\left(\frac{1-n}{1+n}\right)(1 + K_1G''),\ F' = K_1F'' + 1, \\ G' = K_1G'' + A,\ \theta = K_2\theta' + 1, \quad \bar{\varepsilon} = 1 + K_3\bar{\varepsilon}',\ H = 1 + K_4H'. \end{array}\right\}\ at\ \eta \to \alpha_1. \tag{16}$$

$$F' \to 0,\ G' \to 0,\ \theta \to 0,\ \bar{\varepsilon} \to 0,\ H \to 0.\ at\ \eta \to \infty. \tag{17}$$

For the intervals $[0,\ \infty)$, we introduce the following functions,

$$\left.\begin{array}{l} F(\eta) = f(\eta - \alpha_1) = f(\zeta),\ G(\eta) = g(\eta - \alpha_1) = g(\zeta),\ \theta(\eta) = \theta(\eta - \alpha_1) = \theta(\zeta), \\ \bar{\varepsilon}(\eta) = \varepsilon(\eta - \alpha_1) = \varepsilon(\zeta),\ H(\eta) = h(\eta - \alpha_1) = h(\zeta). \end{array}\right). \tag{18}$$

Using equation (18), equation (12–17) takes the following forms,

$$\begin{array}{l} f''' + A_1A_2\left(\frac{n+1}{2}\right)(f+g)f'' - \frac{HaA_2\sigma_{hnf}}{(1+m^2)\sigma_f}(f' + mg') + A_2\lambda(1+\lambda_1\theta)\theta \\ \quad + A_2\lambda N_r(1+\lambda_2\bar{\varepsilon})\bar{\varepsilon} + A_2\lambda N_c(1+\lambda_3H)H - A_1A_2(nf' + ng')f' = 0, \end{array} \tag{19}$$

$$g''' + 2A_1A_2\left(\frac{n+1}{2}\right)\left(\frac{f+g}{2}\right)g'' + \frac{HaA_2\sigma_{hnf}}{(1+m^2)\sigma_f}(mf' - g') - nA_1A_2(f' + g')g' = 0, \tag{20}$$

$$\frac{k_{hnf}}{k_f}\theta'' + \mathrm{Pr}A_3\left[\begin{array}{l}\frac{\sigma_{hnf}HaEc}{\sigma_f A_3\left(1+m^2\right)}\left(f'2 + g'2\right) \\ +\left(\frac{n+1}{2}\right)(f+g)\theta'\end{array}\right] + \frac{\mathrm{Pr}Ec}{A_2}\left(f'2 + g'2\right) = 0, \tag{21}$$

$$\frac{A_2}{S_c}\varepsilon'' + \left(\frac{n+1}{2}\right)(f+g)\varepsilon' - K_r\varepsilon(1+\delta\theta)^{n_1}\exp\left(\frac{-E}{1+\delta\theta}\right) = 0, \tag{22}$$

$$\frac{A_2}{S_b}h'' + \left(\frac{n+1}{2}\right)(f+g)h' - \frac{P_e}{S_b}((h+\Omega)\varepsilon'' + h'\varepsilon') = 0. \tag{23}$$

The concerned boundary condition takes the following form,

$$\left.\begin{array}{l} f = \left(\frac{1-n}{n+1}\right)(\alpha_1 + \alpha_1K_1f''),\ g = \left(\frac{1-n}{n+1}\right)(\alpha_1 + \alpha_1K_1g''),\ f' = 1 + K_1f'', \\ g' = K_1g'' + A,\ \theta = K_2\theta' + 1, \quad \varepsilon = 1 + K_3\varepsilon',\ h = 1 + K_4h'. \end{array}\right\}\ \mathrm{at}\ \zeta \to 0. \tag{24}$$

$$f' \to 0,\ \theta \to 0,\ g' \to 0,\ \varepsilon \to 0,\ h \to 0.\ \mathrm{at}\ \zeta \to \infty. \tag{25}$$

The emerging parameters Ha, λ_1, λ_3, N_r, λ, Ec, λ_2, E, S_c, S_b, P_e, Pr, K_r, δ, α_1, and Ω, which are characterized by Hartmann number, nonlinear convection parameter for temperature, nonlinear convection parameter for microorganism, buoyancy ratio parameter, mixed convection parameter, Eckert number, nonlinear convection parameter for concentration, activation energy parameter, Schmidth number, bio-convection Schmidth number, Peclet number, Prandtl number, chemical reaction parameter, temperature ratio parameter, wall thickness parameter, and microorganism difference parameter respectively. Further, K_1, K_2, K_3, and K_4 are velocity, thermal, concentration, and microorganism slip parameters, respectively. The mathematical form of the parameters is written as,

Table 2
Evaluation of $f''(0)$ and $g''(0)$ with previous data, when $Ha = \alpha_1 = 0 = K_1 = K_2 = \varphi_{1,2}$.

		Nandi et al. [17]		Presents results	
n	A	$f''(0)$	$g''(0)$	$f''(0)$	$g''(0)$
1.00	0.00	−1.000007	0.00000	−1.000008	0.0000
.	0.500	−1.224760	−0.612371	−1.224780	−0.612374
1.00	1.0	−1.414421	−0.414213	−1.4144240	−0.4142150
3.0	0.0	−1.624357	0.00000	−1.624355	0.000000
3.0	0.5	−1.989423	−0.994711	−1.989425	−0.994713
3.0	1.0	−2.2297188	−2.297188	−2.2297186	−2.297186

$$\begin{aligned}
&\mathrm{Pr} = \frac{\nu_f}{\alpha},\ \delta = \frac{T_w}{T_\infty},\ \alpha_1 = j\sqrt{\frac{u_0}{\nu_f}},\ N_r = \frac{Gr_C}{Gr_T},\ Gr_T = \frac{g^*\gamma_3(C_w - C_\infty)(y+x+b)^3}{\nu^2},\ \Omega = \frac{(N_w - N_\infty)}{N_\infty},\\
&Gr_C = \frac{g^*\gamma_1(T_w - T_\infty)(y+x+b)^3}{\nu^2},\ E = \frac{E_a}{T_\infty k_1^*},\ K_r = \frac{K_0^2}{u_0},\ \lambda = \frac{Gr_T}{(\mathrm{Re}_x)^2},\ Ha = \sqrt{\frac{\sigma_f B_0^2}{u_0\rho_f}},\ P_e = \frac{\widetilde{b}W_c}{D_n},\\
&S_c = \frac{\nu_f}{D_B},\ S_b = \frac{\nu_f}{D_n},\ \lambda_1 = \frac{\gamma_2(T_w - T_\infty)}{\gamma_1},\ \lambda_2 = \frac{\gamma_4(T_w - T_\infty)}{\gamma_3},\ \lambda_3 = \frac{\gamma_6(T_w - T_\infty)}{\gamma_5}, Ec = \frac{u_w^2}{(C_p)_f(T_w - T_\infty)},\\
&A_1 = (1-\varphi_1)^{2.5}(1-\varphi_2)^{2.5}, A_2 = \left((1-\varphi_2)\left\{(1-\varphi_1) + \varphi_1\frac{\rho_{MWCNT}}{\rho_f}\right\} + \varphi_2\frac{\rho_{SWCNT}}{\rho_f}\right),\\
&A_3 = \left((1-\varphi_2)\left\{(1-\varphi_1) + \varphi_1\frac{(\rho C_p)_{MWCNT}}{(\rho C_p)_f}\right\} + \varphi_2\frac{(\rho C_p)_{SWCNT}}{(\rho C_p)_f}\right).
\end{aligned} \tag{26}$$

2.3. Physical quantities

The physical quantities like friction drag, heat transport rate, mass transport rate, and microorganism transport rate are very precious for the engineering prospective. These physical interest quantities are defined mathematically as,

$$\begin{aligned}
&Cf_x = \frac{\tau_{xz}}{u_w^2\rho_f},\ Cf_y = \frac{\tau_{yz}}{v_w^2\rho_f}, Nu_x = \frac{(x+y+b)q_m}{k_f(T_w - T_\infty)},\\
&Sh_x = \frac{(x+y+b)j_m}{(D_B)_f(C_w - C_\infty)}, Qn_x = \frac{(x+y+b)z_w}{(D_n)_f(N_w - N_\infty)},
\end{aligned} \tag{27}$$

In equation (27) τ_{xz}, τ_{yz}, q_m, j_m, and z_w are defined as,

$$\begin{aligned}
&\tau_{xz} = \mu_{hnf}\left|\frac{\partial u}{\partial z}\right|_{z=j(b+y+x)^{\frac{1-n}{2}}},\ \tau_{xz} = \mu_{hnf}\left|\frac{\partial v}{\partial z}\right|_{z=j(b+y+x)^{\frac{1-n}{2}}},\ q_m = -\left|k_{hnf}\frac{\partial T}{\partial z}\right|_{z=j(b+y+x)^{\frac{1-n}{2}}},\\
&j_m = -(D_B)_{hnf}\left|\frac{\partial C}{\partial z}\right|_{z=j(b+y+x)^{\frac{1-n}{2}}},\ z_w = -(D_n)_{hnf}\left|\frac{\partial N}{\partial z}\right|_{z=j(b+y+x)^{\frac{1-n}{2}}}.
\end{aligned} \tag{28}$$

In the dimensionless form these are written as,

$$\begin{aligned}
&(\mathrm{Re}_x)^{0.5}Cf_x = 2\left(\frac{n+1}{2}\right)^{0.5}\frac{f''(0)}{(1-\varphi_1)^{2.5}(1-\varphi_2)^{2.5}},\ (\mathrm{Re}_y)^{0.5}Cf_y = 2\left(\frac{n+1}{2}\right)^{0.5}\frac{g''(0)}{(1-\varphi_1)^{2.5}(1-\varphi_2)^{2.5}},\\
&Nu_x(\mathrm{Re}_x)^{-0.5} = -\left(\frac{n+1}{2}\right)^{0.5}\frac{k_{hnf}}{k_f}\theta'(0),\ Sh_x(\mathrm{Re}_x)^{-0.5} = \left(\frac{n+1}{2}\right)^{0.5}(1-\varphi_1)^{2.5}(1-\varphi_2)^{2.5}\varepsilon'(0),\\
&Qn_x(\mathrm{Re}_x)^{-0.5} = \left(\frac{n+1}{2}\right)^{0.5}(1-\varphi_1)^{2.5}(1-\varphi_2)^{2.5}h'(0).
\end{aligned} \tag{29}$$

$\mathrm{Re}_x = \frac{(b+y+x)u_w}{\nu}$ and $\mathrm{Re}_y = \frac{(b+y+x)v_w}{\nu}$ is the Reynolds number.

3. Results and discussion

The bvp4c numerical technique is used to answer Eqs. 12–15 with Eq (16). For numerous developing parameters, the graphical results are achieved for velocity, microorganism, concentration, and temperature distribution. Moreover, the result of nanofluid $SWCNT - C_2H_2F_4$ and hybrid nanofluid $SWCNT - MWCNT - C_2H_2F_4$ are compared and discussed. The emerging parameters range has been signified as $\alpha_1 = (0 - 1.0), Ha = (0 - 3.0), K_1 = K_2 = K_3 = K_4 = (0 - 1.0), \lambda = (0 - 1.0), S_c = (1.0 - 4.0), E = (0 - 1.5)$, $K_r = (0 - 1.0)$, $\varphi_2 = \varphi_1 = (0.0 - 0.05)$, $P_e = (0.1 - 1.0)$, and $S_b = (1.0 - 4.0)$. The comparison of current problem with earlier

Table 3
Numerical values of $-Cf_x\mathrm{Re}_x^{0.5}$ and $-Cf_y\mathrm{Re}_y^{0.5}$ against the various parameters.

α_1	φ_1	K_1	n	λ	$-Cf_x\mathrm{Re}_x^{0.5}$		$-Cf_y\mathrm{Re}_y^{0.5}$	
					Simple nanofluid ($\varphi_2 = 0$)	Hybrid nanofluid ($\varphi_2 = 0.03$)	Simple nanofluid ($\varphi_2 = 0$)	Hybrid nanofluid ($\varphi_2 = 0.03$)
0.2	0.01	0.5	0.3	0.5	0.49483	0.52983	0.36206	0.38382
0.3					0.53822	0.57076	0.37207	0.39411
0.4					0.57638	0.60763	0.38158	0.40399
	0.02				0.50490	0.54041	0.36844	0.39046
	0.03				0.51514	0.55117	0.37500	0.39730
	0.05				0.52557	0.56213	0.38174	0.40433
		0.1			0.74357	0.78367	0.55614	0.57702
		1.5			0.20619	0.23658	0.15713	0.19916
		3.0			0.10475	0.13572	0.09362	0.11968
			0.1		0.38125	0.40335	0.27602	0.30811
			0.5		0.47342	0.50139	0.33129	0.36567
			0.7		0.50241	0.53495	0.35156	0.38125
				0.1	0.70123	0.73127	0.33245	0.36431
				0.3	0.63523	0.65125	0.31722	0.35543
				0.5	0.51345	0.52917	0.30125	0.33175

Table 4
Numerical values of $\mathrm{Re}_x^{-1/2}Nu_x$ for several parameters.

λ	n	E_c	φ_1	K_2	Ha	$\mathrm{Re}_x^{-1/2}Nu_x$	
						Simple nanofluid ($\varphi_2 = 0.0$)	Hybrid nanofluid ($\varphi_2 = 0.03$)
0.1	0.3	1.0	0.01	0.5	0.1	0.58467	0.68551
0.3						0.68282	0.77034
0.5						0.82366	0.92823
	0.3					0.45915	0.55735
	0.4					0.42521	0.52320
	0.5					0.40163	0.50251
		0.2				0.42319	0.53321
		0.3				0.26618	0.37518
		0.4				0.21441	0.32513
			0.02			0.85825	0.96334
			0.03			0.89270	0.99816
			0.04			0.92722	1.03300
				0.2		1.11620	1.20890
				0.4		0.90254	1.00610
				0.6		0.75744	0.86152
					0.1	0.75744	0.86152
					0.3	1.04800	1.20290
					0.5	1.23060	1.41640

Table 5
Numerical values of $\mathrm{Re}_x^{-1/2}Sh_x$ for several parameters.

φ_1	n	S_c	δ	K_3	K_r	$\mathrm{Re}_x^{-1/2}Sh_x$	
						Simple nanofluid ($\varphi_2 = 0.0$)	Hybrid nanofluid ($\varphi_2 = 0.03$)
0.02	0.3	3.0	1.0	0.5	1.0	1.1184	1.2363
0.03						1.1569	1.2785
0.04						1.1970	1.3223
	0.3					1.1966	1.3531
	0.4					1.1959	1.3580
	0.5					1.1947	1.3599
		2.0				1.1968	1.3179
		2.5				1.1962	1.3173
		2.9				1.1949	1.3160
			0.2			1.1326	1.2526
			0.3			1.1653	1.2853
			0.4			1.1933	1.3033
				1.0		1.5193	1.6315
				1.5		1.3735	1.4864
				2.0		1.2277	1.3413

Table 6
Numerical data of $\mathrm{Re}_x^{-1/2}Nn_x$ for numerous parameters.

φ_1	N_c	N_r	S_b	K_4	$\mathrm{Re}_x^{-1/2}Qn_x$	
					Simple nanofluid ($\varphi_2 = 0.0$)	Hybrid nanofluid ($\varphi_2 = 0.03$)
0.02	0.1	0.1	0.1	0.1	1.09860	1.23250
0.03					1.14231	1.28112
0.04					1.18801	1.33190
	0.3				1.10492	1.24482
	0.4				1.10433	1.24425
	0.5				1.10375	1.24374
		0.2			1.18454	1.33462
		0.3			1.18403	1.33401
		0.4			1.18362	1.33365
			0.2		1.16521	1.28521
			0.3		1.18963	1.30961
			0.4		1.20362	1.32361
				1.0	1.15358	1.33358
				1.5	1.10680	1.26680
				2.0	1.05045	1.20002

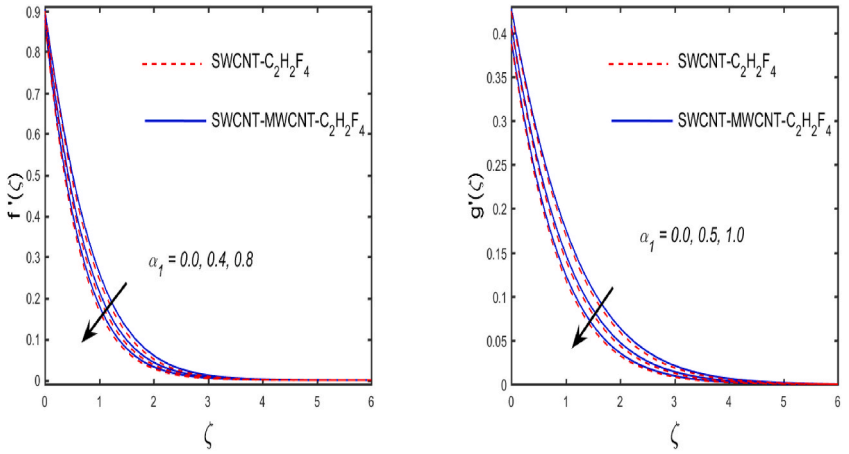

(a) **(b)**

Fig. 2. (a and b): Variation in $f'(\zeta)$ and $g'(\zeta)$ for α_1.

publish results is presented in Table 2. It is noticed that higher values of A improved the velocity gradient ($f''(0)$ and $g''(0)$). Tables 3–6 shows the numerical values of skin friction along x and y-axis, heat transport rate, Sherwood number, and microorganism number respectively.

The effect of α_1 (wall thickness parameter), Ha (Hartmann number), K_1 (parameter of velocity slip), K_2 (parameter of thermal slip), K_3 (parameter of concentration slip), λ (mixed convection parameter), S_c (Schmidt number), E (parameter of activation energy), K_r (parameter of chemical reaction), φ_2 (solid volume fraction parameter) on the $f'(\zeta)$, $g'(\zeta)$, $\theta(\zeta)$, $\varepsilon(\zeta)$, and $h(\zeta)$ is discussed in Figs. (2 – 8). It is deliberated in Fig. 2(a and b) that by the increment of wall thickness the parameter the momentum boundary layer thickness reduces for both nanofluid and hybrid nanofluid, therefore the velocity of the fluid declined in both directions. Physically, when increases the estimation of α_1 it performs as a retarding factor, due to this the fluid velocity retard. The variation in $f'(\zeta)$ and $g'(\zeta)$ plots for various estimation of K_1 for $SWCNT - C_2H_2F_4$ and $SWCNT - MWCNT - C_2H_2F_4$ is portrayed in Fig. 3(a and b). It illustrates that both velocities ($f'(\zeta)$ and $g'(\zeta)$) are slow down along the boundary of the surface but shows opposite trend away from the surface, due to the increment of K_1. This shows that slip velocity parameter has a propensity to improve the velocity away from the sheet (wall) and revers trend is noted near the wall. Fig. 4(a – e) demonstrates the impact of φ_2 on the velocity sketch ($f'(\zeta)$ and $g'(\zeta)$), temperature field ($\theta(\zeta)$), concentration profile ($\varepsilon(\zeta)$), and microorganism field ($h(\zeta)$) for both $SWCNT - C_2H_2F_4$ and $MWCNT - SWCNT - C_2H_2F_4$. It is obvious from the figure that both $f'(\zeta)$ and $g'(\zeta)$ improves with the escalation of φ_2. From Fig. 4(c) is noted that the thermal conductivity of fluid boosts by the inclusion of the hybrid nanofluid, this implies that the temperature of fluid is improved by the escalation of φ_2. Further, Fig. 4(d and e) shows that concentration and microorganism of fluid is diminished as growing the values of φ_2. Fig. 4(f and g) demonstrate the comparison of simple nanofluid and hybrid nanofluid for velocity and temperature of fluid flow. It is seen that the velocity, as well as temperature profile, show good behavior for hybrid nanofluid than simple nanofluid. The variation in the $f'(\zeta)$,

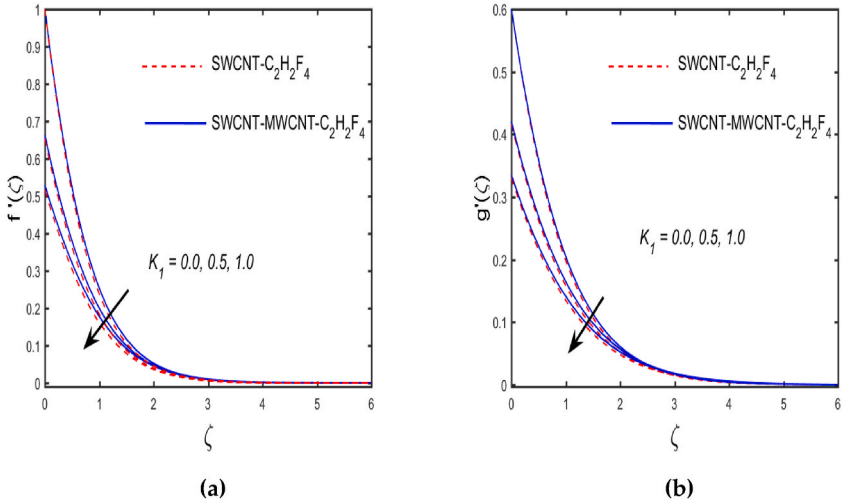

Fig. 3. (a and b): Variation in $f'(\zeta)$ and $g'(\zeta)$ for K_1.

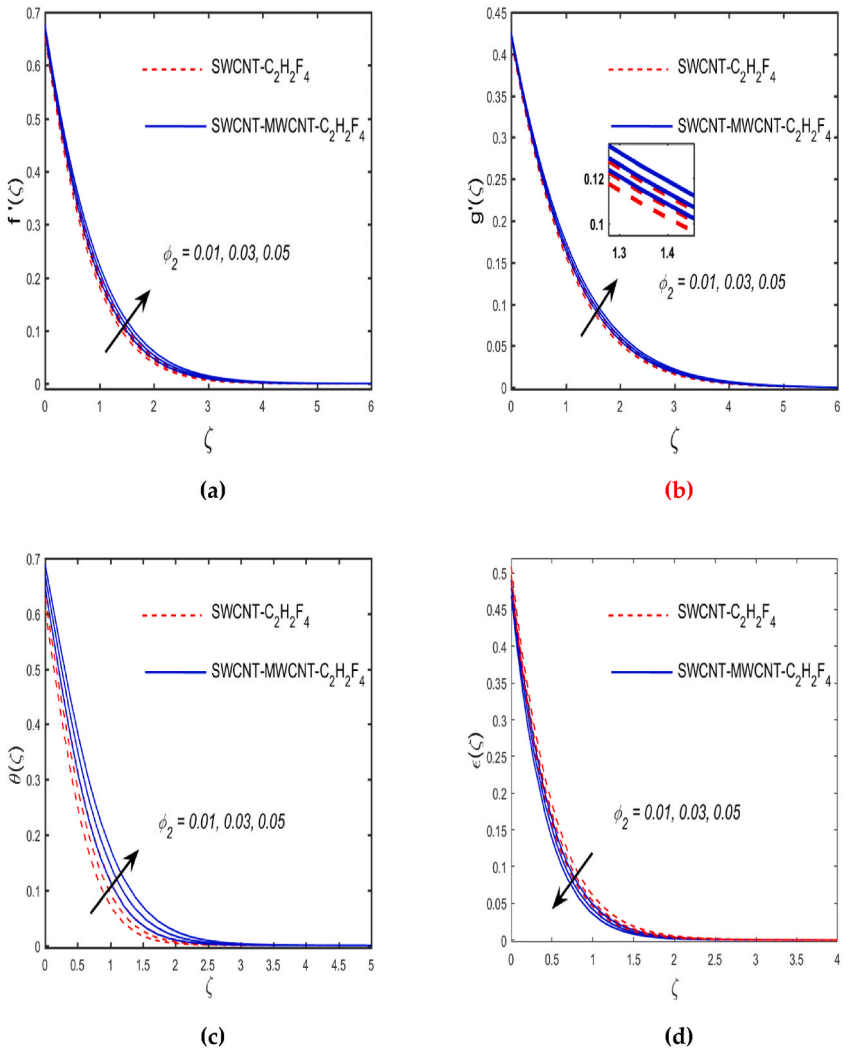

Fig. 4. (a–g): Variation in $f'(\zeta)$, $g'(\zeta)$, $\theta(\zeta)$, $\varepsilon(\zeta)$, and $h(\zeta)$ for φ_2.

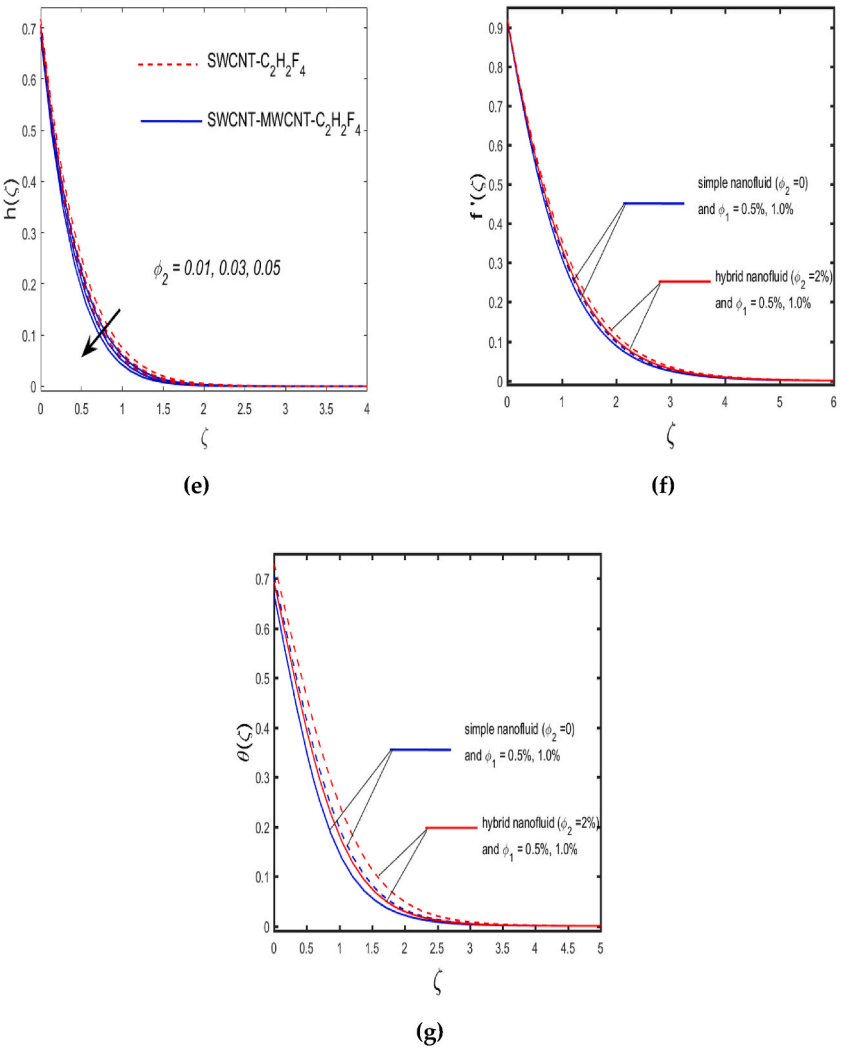

Fig. 4. (*continued*).

$g'(\zeta)$ and $\theta(\zeta)$ plots against the several values of Ha are displayed in Fig. 5(a – c). It demonstrates that the fluid velocity in both directions ($f'(\zeta)$ and $g'(\zeta)$) are depreciated by the enhancement of the Hartmann number for both cases. Physically, due to increment of Hartmann number the retardation effect take place, thereby the velocity of the fluid shrinks while the temperature distribution enhances (see in Fig. 5(c)). Fig. 6(a and b) shows the impact of parameter of mixed convection on the velocity field ($f'(\zeta)$ and $g'(\zeta)$) for both cases. The figure shows that the reduction is occurred in $f'(\zeta)$ and enhancement in $g'(\zeta)$ by the increment of λ. Physically, the viscous forces are dominated by the escalation of λ, therefore the fluid velocity in $x-$ direction reduces, while in $y-$ direction velocity is enlarged. Fig. 6(c) shows the influence of E on the concentration plot. It is investigated that the stronger values of E raises the concentration sketch. The physics behind this is that due stronger activation energy more energy is transmitted surface to the fluid, due to this the nanoparticles concentration and temperature of fluid enlargers. Fig. 6(d) depicts the effect of Schmidt number on the concentration sketch. It is noticed that the concentration sketch declines due to the higher estimation of S_c for $SWCNT- C_2H_2F_4$ and $MWCNT - SWCNT - C_2H_2F_4$. Physically, due higher values of S_c, the mass diffusivity of fluid decreases, as a result the concentration of fluid is declined. Aspect of thermal and concentration slip parameter on the temperature and concentration distribution is described in Fig. 7(a and b). It is explored from the sketch that $\theta(\zeta)$ and $\varepsilon(\zeta)$ plots declines by the improving values of K_2 and K_3 for $SWCNT- C_2H_2F_4$ and $MWCNT - SWCNT - C_2H_2F_4$. Physically, by boosting the values of K_2, the thermal diffusion rate in the direction flow is decreased, thereby the fluid temperature is decayed. The results of K_4 on the microorganism distribution is presented in Fig. 7(c). It evidences from the figure that by the enhancement of K_4, the $h(\zeta)$ plot is devalued for both nanofluid and hybrid nanofluid. It is obvious from Fig. 8(a and b) that the reduction arises in the microorganism density profile and associated boundary layer thickness due to growing values of P_e and S_b for both simple and hybrid nanofluid. Physically, stronger values of P_e improves the cell swimming speed and decreases the microorganism diffusivity, as a result microorganism density profile is decayed. Moreover, microorganism diffusion rate shrinks due to growth of S_b, which shows that microorganism profile is reduced.

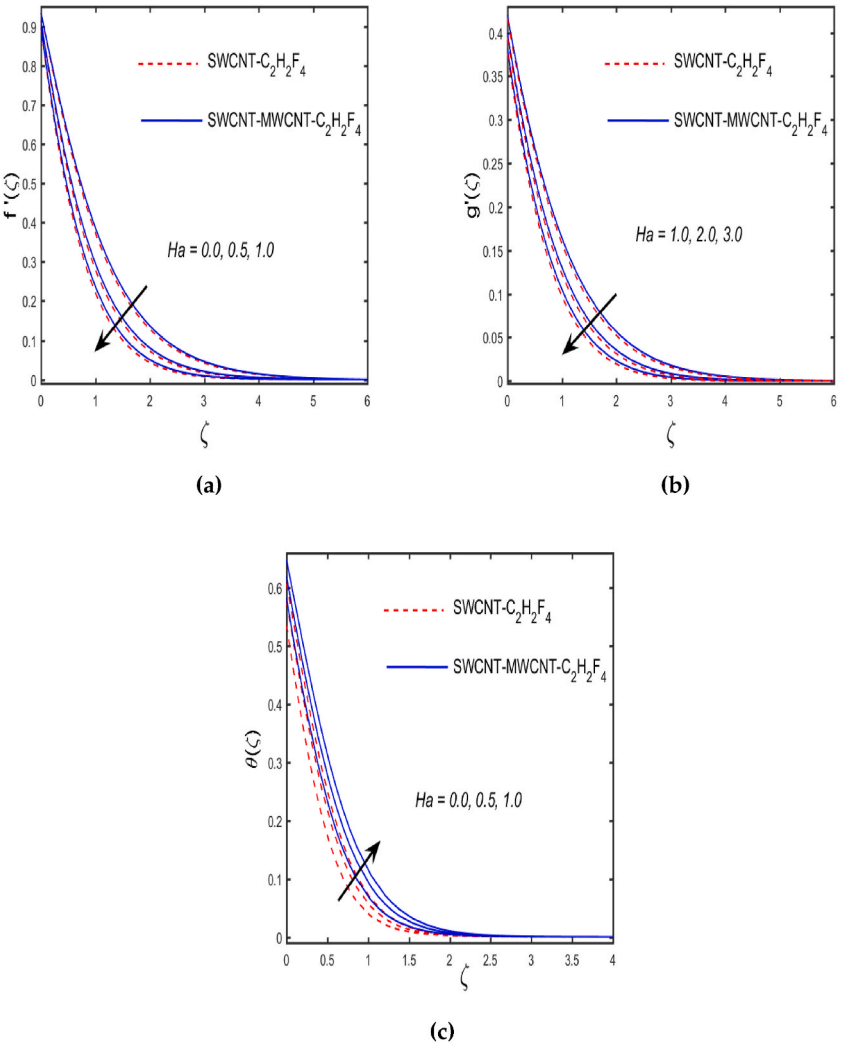

Fig. 5. (a–c): Variation in $f^{'}(\zeta)$, $g^{'}(\zeta)$, and $\theta(\zeta)$ for Ha.

4. Concluding remarks

The nonlinear mixed convective viscous boundary layer flow of radiating hybrid nanofluid flow with the existence of activation energy, joule heating, and microorganism is presented. The multiple slip conditions are imposed on the boundary of the slendering surface. The $SWCNT-MWCNT-C_2H_2F_4$ cases for hybrid nanofluid using *CNTs* is discussed. The mathematical model is converted into ODEs and using bvp4c Matlab technique to solve these ODEs. The main outcomes of the paper are illustrated as follows:

- The stronger values of α_1 provided the retardation effect which declines the fluid velocity for both $SWCNT-C_2H_2F_4$ and $MWCNT-SWCNT-C_2H_2F_4$ cases.
- By the increment of λ the viscous forces are dominated, as a result the fluid velocity improves for both $SWCNT-C_2H_2F_4$ and $MWCNT-SWCNT-C_2H_2F_4$.
- The larger values of φ_2 improving the fluid velocity and thickness of momentum boundary layer.
- The higher values of Ha and n, the retardation effect take places, as a result the fluid temperature enlarges for both $SWCNT-C_2H_2F_4$ and $MWCNT-SWCNT-C_2H_2F_4$.
- The growing values of P_e and S_b declines the microorganism diffusion rate, as a result the $h(\zeta)$ profile for both $SWCNT-C_2H_2F_4$ and $MWCNT-SWCNT-C_2H_2F_4$ diminishes.
- By the enhancement α_1, the drag friction in both ($x-$ and $y-$) directions are enlarged, while opposite trend is noted in case of mixed convection parameter.
- The heat transfer rate decreases for the larger estimation of Ec.
- The mass transfer rate improves due to the improvement of K_r.
- The higher values of mixed convection parameter improve the microorganism transfer rate.

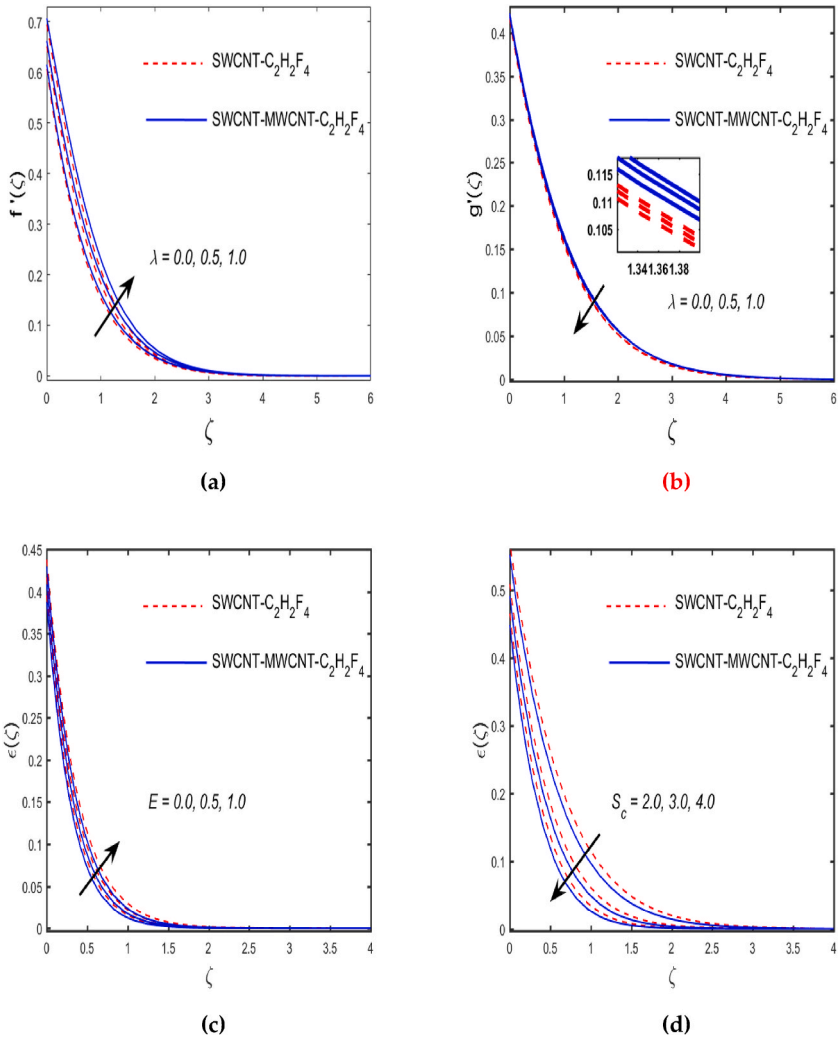

Fig. 6. (a–d): Variation in $f'(\zeta)$ and $g'(\zeta)$ for λ and $\varepsilon(\zeta)$ for E and S_c.

Funding

This research work was supported by the Deanship of Scientific Research at King Khalid University under Grant number RGP. 1/155/42.

Author statement

Wei-Feng Xia: Methodology, Conceptualization, Writing- Review and editing.
Shafiq Ahmad: Methodology, Validation, Software, Conceptualization, Writing- Original draft.
Muhammad Naveed Khan: Methodology, Software, Investigation, Conceptualization, Writing- Original draft.
Hijaz Ahmad: Methodology, Software, Validation, Investigation, Conceptualization, Writing- Original draft.
Aysha Rehma: Supervision, Validation, Investigation, Validation, Writing-Review and editing.
Jamel Baili: Software, Investigation, Validation, Writing-Review and editing.
Tuan Nguyen Gia: Supervision, Funding, Conceptualization, Writing- Review and editing.

Declaration of competing interest

The authors declare that they have no known competing financial interests or personal relationships that could have appeared to influence the work reported in this paper.

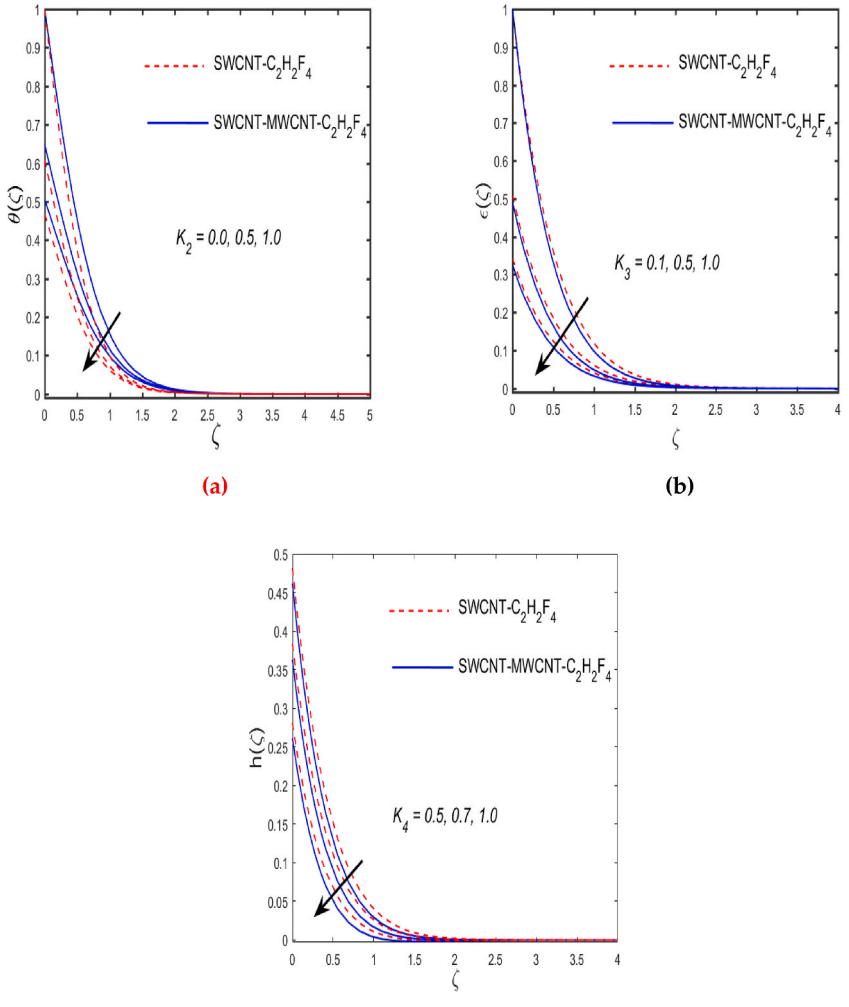

Fig. 7. (a–c): Variation in $\theta(\zeta)$ for K_2, $\varepsilon(\zeta)$ for K_3 and $h(\zeta)$ for.K_4.

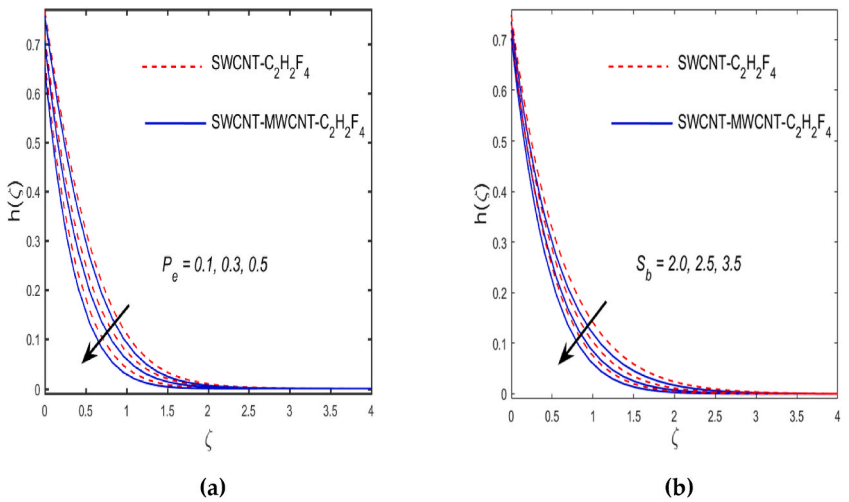

Fig. 8. (a and b): Variation in $h(\zeta)$ for P_e and S_b.

Acknowledgements

The Authors extend their thanks to the Deanship of Scientific Research at King Khalid University, Saudi Arabia for funding this work through the big research groups under grant number RGP. 1/155/42.

References

[1] S. Hofmann, R. Sharma, C. Ducati, G. Du, C. Mattevi, C. Cepek, M. Cantoro, S. Pisana, A. Parvez, F. Cervantes-Sodi, A.C. Ferrari, In situ observations of catalyst dynamics during surface-bound carbon nanotube nucleation, Nano Lett. 7 (3) (2007) 602–608.
[2] U. Khan, N. Ahmed, S.T. Mohyud-Din, Numerical investigation for three-dimensional squeezing flow of nanofluid in a rotating channel with lower stretching wall suspended by carbon nanotubes, Appl. Therm. Eng. 113 (2017) 1107–1117.
[3] T. Hayat, F. Haider, T. Muhammad, A. Alsaedi, On Darcy-Forchheimer flow of carbon nanotubes due to a rotating disk, Int. J. Heat Mass Tran. 112 (2017) 248–254.
[4] I. Shahzadi, H. Sadaf, S. Nadeem, A. Saleem, Bio-mathematical analysis for the peristaltic flow of single wall carbon nanotubes under the impact of variable viscosity and wall properties, Comput. Methods Progr. Biomed. 139 (2017) 137–147.
[5] A.R. Rahmati, M. Reiszadeh, An experimental study on the effects of the use of multi-walled carbon nanotubes in ethylene glycol/water-based fluid with indirect heaters in gas pressure reducing stations, Appl. Therm. Eng. 134 (2018) 107–117.
[6] R. Ramasubramaniam, J. Chen, H. Liu, Homogeneous carbon nanotube/polymer composites for electrical applications, Appl. Phys. Lett. 83 (14) (2003) 2928–2930.
[7] Q.Z. Xue, Model for thermal conductivity of carbon nanotube-based composites, Phys. B Condens. Matter 368 (1–4) (2005) 302–307.
[8] R.K. Kumar, S.V.K. Varma, C.S.K. Raju, S.M. Ibrahim, G. Lorenzini, E. Lorenzini, Retracted article: magnetohydrodynamic 3D slip flow in a suspension of carbon nanotubes over a slendering sheet with heat source/sink, Continuum Mech. Therm. 29 (3) (2017) 835–851.
[9] S. Manjunatha, B.A. Kuttan, G.K. Ramesh, B.J. Gireesha, E.H. Aly, 3D flow and heat transfer of micropolar fluid suspended with mixture of nanoparticles (Ag-CuO/H2O) driven by an exponentially stretching surface, Multidiscip. Model. Mater. Struct. 16 (6) (2020) 1691–1707.
[10] G.K. Ramesh, S. Manjunatha, G.S. Roopa, A.J. Chamkha, Hybrid (ND-Co 3 O 4/EG) nanoliquid through a permeable cylinder under homogeneous-heterogeneous reactions and slip effects, J. Therm. Anal. Calorim. (2020) 1–11.
[11] V. Puneeth, S. Manjunatha, B.J. Gireesha, R.S.R. Gorla, Magneto convective flow of casson nanofluid due to Stefan blowing in the presence of bio-active mixers, in: Proceedings of the Institution of Mechanical Engineers, Part N: Journal of Nanomaterials, Nanoengineering and Nanosystems, 2021, 23977914211016692.
[12] M.N. Khan, S. Ahmad, S. Nadeem, Flow and heat transfer investigation of bio–convective hybrid nanofluid with triple stratification effects, Phys. Scripta 96 (6) (2021), 065210.
[13] V. Puneeth, S. Manjunatha, B.J. Gireesha, Quartic autocatalysis of homogeneous and heterogeneous reactions in the bioconvective flow of radiating micropolar nanofluid between parallel plates, Heat Transf. 50 (6) (2021) 5925–5950.
[14] A. Saleem, S. Akhtar, S. Nadeem, M. Ghalambaz, Microphysical analysis for peristaltic flow of SWCNT and MWCNT carbon nanotubes inside a catheterised artery having thrombus: irreversibility effects with entropy, Int. J. Exergy 34 (3) (2021) 301–314.
[15] T. Hayat, M. Khan, M.I. Khan, A. Alsaedi, M. Ayub, Electromagneto squeezing rotational flow of Carbon (C)-Water (H2O) kerosene oil nanofluid past a Riga plate: a numerical study, PLoS One 12 (8) (2017), e0180976.
[16] .
[17] M.J. Babu, N. Sandeep, MHD non-Newtonian fluid flow over a slendering stretching sheet in the presence of cross-diffusion effects, Alex. Eng. J. 55 (3) (2016) 2193–2201.
[18] S. Nandi, B. Kumbhakar, G.S. Seth, A.J. Chamkha, Features of 3D magneto-convective nonlinear radiative Williamson nanofluid flow with activation energy, multiple slips and Hall effect, Phys. Scripta 96 (6) (2021), 065206.
[19] S.P. Devi, M. Prakash, Slip flow effects over hydromagnetic forced convective flow over a slendering stretching sheet, J. Appl. Fluid Mech. 9 (2) (2016).
[20] M.T. Akolade, A.S. Idowu, A.T. Adeosun, Multislip and Soret–Dufour influence on nonlinear convection flow of MHD dissipative Casson fluid over a slendering stretching sheet with generalized heat flux phenomenon, Heat Transf. 50 (4) (2021) 3913–3933.
[21] S. Qayyum, T. Hayat, A. Alsaedi, Thermal radiation and heat generation/absorption aspects in third grade magneto-nanofluid over a slendering stretching sheet with Newtonian conditions, Phys. B Condens. Matter 537 (2018) 139–149.
[22] J.R. Reddy, V. Sugunamma, N. Sandeep, Effect of frictional heating on radiative ferrofluid flow over a slendering stretching sheet with aligned magnetic field, Euro. Phys. J. Plus 132 (1) (2017) 1–13.
[23] M.J. Babu, N. Sandeep, Three-dimensional MHD slip flow of nanofluids over a slendering stretching sheet with thermophoresis and Brownian motion effects, Adv. Powder Technol. 27 (5) (2016) 2039–2050.
[24] N. Acharya, K. Das, P.K. Kundu, Ramification of variable thickness on MHD TiO 2 and Ag nanofluid flow over a slendering stretching sheet using NDM, Euro. Phys. J. Plus 131 (9) (2016) 1–16.
[25] M. Prakash, S. Devi, Hydromagnetic hybrid Al2O3-Cu/water nanofluid flow over a slendering stretching sheet with prescribed surface temperature, Asian J. Res. Soc. Sci. Humanit. 6 (9) (2016) 1921–1936.
[26] G.V. Kumar, R.K. Kumar, S.V.K. Varma, Unsteady magnetohydrodynamic stagnation point flow of a nanofluid over a slendering stretching sheet using Buongiorno's model, Int J Res Ind Eng 7 (1) (2018) 84–105.
[27] C. Sulochana, N. Sandeep, Dual solutions for radiative MHD forced convective flow of a nanofluid over a slendering stretching sheet in porous medium, J. Nav. Architect. Mar. Eng. 12 (2) (2015) 115–124.
[28] A. Moradi, H. Ahmadikia, T. Hayat, A. Alsaedi, On mixed convection–radiation interaction about an inclined plate through a porous medium, Int. J. Therm. Sci. 64 (2013) 129–136.
[29] S. Ahmad, S. Nadeem, M.N. Khan, Mixed convection hybridized micropolar nanofluid with triple stratification and Cattaneo–Christov heat flux model, Phys. Scripta 96 (7) (2021), 075205.
[30] E.M. Elsaid, M.S. Abdel-wahed, Mixed convection hybrid-nanofluid in a vertical channel under the effect of thermal radiative flux, Case Stud. Therm. Eng. 25 (2021) 100913.
[31] V. Puneeth, S. Manjunatha, O.D. Makinde, B.J. Gireesha, Bioconvection of a radiating hybrid nanofluid past a thin needle in the presence of heterogeneous–homogeneous chemical reaction, J. Heat Tran. 143 (4) (2021), 042502.
[32] S. Nadeem, S. Ahmad, M.N. Khan, Mixed convection flow of hybrid nanoparticle along a Riga surface with Thomson and Troian slip condition, J. Therm. Anal. Calorim. 143 (2021) 2099–2109.
[33] M.G. Reddy, K.V. Reddy, Influence of Joule heating on MHD peristaltic flow of a nanofluid with compliant walls, Procedia Eng. 127 (2015) 1002–1009.
[34] T. Hayat, S.A. Khan, A. Alsaedi, Q.Z. Zia, Irreversibility analysis in Darcy-Forchheimer flow of CNTs with dissipation and Joule heating effects by a curved stretching sheet, Appl. Nanosci. 11 (1) (2021) 187–198.
[35] S.S. Ghadikolaei, K. Hosseinzadeh, D.D. Ganji, Numerical study on magneto hydrodynic CNTs-water nanofluids as a micropolar dusty fluid influenced by non-linear thermal radiation and joule heating effect, Powder Technol. 340 (2018) 389–399.
[36] M. Shoaib, M.A.Z. Raja, M.T. Sabir, M. Awais, S. Islam, Z. Shah, P. Kumam, Numerical analysis of 3-D MHD hybrid nanofluid over a rotational disk in presence of thermal radiation with Joule heating and viscous dissipation effects using Lobatto IIIA technique, Alex. Eng. J. 60 (4) (2021) 3605–3619.
[37] M. Ijaz, M. Yousaf, A.M. El Shafey, Arrhenius activation energy and Joule heating for Walter-B fluid with Cattaneo–Christov double-diffusion model, J. Therm. Anal. Calorim. 143 (5) (2021) 3687–3698.

[38] M.I. Khan, S. Qayyum, T. Hayat, M.I. Khan, A. Alsaedi, Entropy optimization in flow of Williamson nanofluid in the presence of chemical reaction and Joule heating, Int. J. Heat Mass Tran. 133 (2019) 959–967.
[39] M.I. Khan, F. Alzahrani, Binary chemical reaction with activation energy in dissipative flow of non-Newtonian nanomaterial, J. Theor. Comput. Chem. 19 (2020) 2040006, 03.
[40] M.I. Khan, F. Alzahrani, A. Hobiny, Z. Ali, Fully developed second order velocity slip Darcy-Forchheimer flow by a variable thicked surface of disk with entropy generation, Int. Commun. Heat Mass Tran. 117 (2020) 104778.
[41] S. Ahmad, S. Nadeem, M.N. Khan, Enhanced transport properties and its theoretical analysis in two-phase hybrid nanofluid, Appl. Nanosci. (2021) 1–8.
[42] T. Hayat, M.I. Khan, M. Tamoor, M. Waqas, A. Alsaedi, Numerical simulation of heat transfer in MHD stagnation point flow of Cross fluid model towards a stretched surface, Results Phys. 7 (2017) 1824–1827.
[43] S. Ahmad, S. Nadeem, Hybridized nanofluid with stagnation point past a rotating disk, Phys. Scripta 96 (2) (2020), 025214.